IEEE Access
Multidisciplinary | Rapid Review | Open Access Journal

Received September 9, 2019, accepted October 14, 2019, date of publication October 21, 2019, date of current version November 1, 2019.

Digital Object Identifier 10.1109/ACCESS.2019.2948781

Experimental Development of a Health Monitoring Method for Electro-Mechanical Actuators of Flight Control Primary Surfaces in More Electric Aircrafts

MIRKO MAZZOLENI[1], (Member, IEEE), FABIO PREVIDI[1], (Member, IEEE), MATTEO SCANDELLA[1], AND GIULIO PISPOLA[2]

[1]Department of Management, Information and Production Engineering, University of Bergamo, 24044 Dalmine, Italy
[2]Umbra Group S.p.A., 06034 Foligno, Italy

Corresponding author: Mirko Mazzoleni (mirko.mazzoleni@unibg.it)

This work was supported by the European Union's Horizon 2020 Research and Innovation Programme through the Clean Sky 2 Joint Technology Initiative (JTI-CS2-2015-CFP02-SYS-03-01) under Grant 717112 (project acronym: REPRISE).

ABSTRACT This paper presents a health monitoring approach for Electro-Mechanical Actuators (EMA). We define four different indicators to continuously evaluate the health state of the system. The four indicators are computed by leveraging the output from a Statistical Process Monitoring (SPM) method based on multivariate statistics, such as the Hotelling's T^2 statistic and the Q statistic. SPM approaches give a dichotomous answer, i.e. the presence/absence of a fault. In this work, we propose four ways to compute a continuous indicator starting from the discrete SPM output, that is better suited for health monitoring. We test the approach using a dataset collected from a large experimental campaign on a 1:1 scale EMA for primary flight controls of small aircrafts, that led to EMA failure. Results show the effectiveness of the method.

INDEX TERMS Actuators, aerospace components, aerospace safety, condition monitoring, electromechanical systems, fault detection, predictive maintenance, statistical process monitoring.

I. INTRODUCTION

The More/All Electric Aircraft (MEA/AEA) initiative is a technological trend aiming to increase the adoption of electrical actuation systems in the aerospace field [1], [2]. In this context, we talk about Power-By-Wire (PBW) technology, referring to the elimination of the hydraulic transmission in flight control actuation systems (see Fig. 1).

Traditional actuation equipment on aircrafts rely on hydraulic systems [3]. In PBW actuation, instead, hydraulic pipelines are replaced by electrical wires. PBW actuators benefit aircrafts actuation systems with a series of advantages. These include the reduction of hydraulic fluids, weight savings and improved energy efficiency [1], [4], [5]. PBW solutions consist of: (i) Electro-HydroStatic Actuators (EHSAs) [6] and (ii) Electro-Mechanical Actuators (EMAs) [4], see Fig. 2.

The associate editor coordinating the review of this manuscript and approving it for publication was Kan Liu.

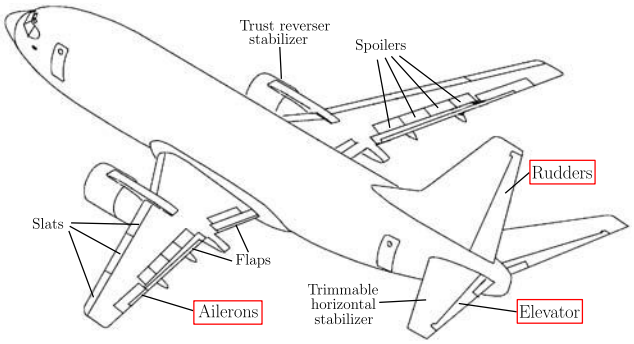

FIGURE 1. Flight control surfaces. Primary controls are highlighted.

Several research programs have been launched in order to investigate the advantages of electro-mechanical actuation systems in aerospace. Some of these, focused on primary controls, include (in chronological order): the Advanced Electromechanical Actuation System (EMAS) [7],

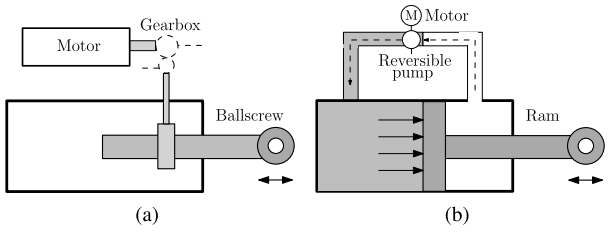

FIGURE 2. EMA (Gear-drive) vs EHSAs.

the Electrically Powered Actuation Design (EPAD) [8], the Power Optimised Aircraft (POA)-FP5 [9], the More Open Electrical Technologies (MOET)-FP6 [10], the flight control with distributed intelligence and systems integration (COVADIS) [11], and the ACTUATION2015-FP7 [12] projects. Research on secondary control actuation has been faced, as illustrative example, in the Distributed Electrically Actuated Wing System (DEAWS) project [13].

After these researches, EMAs started to be deployed to in-service aircrafts [2]. For instance, EMAs are used for landing gear braking, mid spoiler surfaces and trimmable horizontal stabilizer on Boeing 787 [14]. On Airbus A380, EHSAs are employed for ailerons and elevators, while EMAs are utilized for slats, trimmable horizontal stabilizer and thrust reverser actuation [15]. Electro-mechanical actuators are employed also for the following applications: propeller brake system (Airbus A400M), cart lift system (Boeing 747-8, Boeing 777-300), and pedestal radar actuation (Agusta NH-90).

Nevertheless, compared to hydraulic actuators or EHSAs, technological barriers remain for a *wide adoption* of EMAs, especially considering these issues:

- It is difficult to provide space for EMAs on thin wings of small aircrafts, i.e. maximum gross takeoff weight of 5.670 kg (12.500 lb) or less [16].
- The use of EMAs for flight control surfaces requires an optimisation effort in terms of materials, sensors, heat dissipation and electrical distribution [17], [18].
- Mechanical jams cannot be tolerated in flight-critical applications.

The last point raised a critical issue. The lack of accumulated knowledge and experience regarding reliability, and the risk of failure due to jamming of the mechanical transmission (usually a ballscrew), drove significant research efforts towards the development of Fault Diagnosis (FD) and Health Monitoring (HM) algorithms for EMAs in aerospace.

This paper presents a part of the results of the Reliable Electromechanical actuator for PRImary SurfacE with health monitoring (REPRISE) initiative, a EU-H2020 funded project that aims at introducing HM algorithms for *primary flight control surfaces EMAs* in small aircrafts (aileron, elevator and rudder) [19]. The scope of the REPRISE project is to support the improvement of the Technological Readiness Level (TRL) for a EMA-based flight control system of small aircrafts bringing it to TRL 5. The goal of the project will be achieved by:

1) Developing a Health Monitoring system (*Phase 1*).
2) Design a new electro-mechanical actuator architecture (*Phase 2*).

This paper is focused on the results of the first activity (*Phase 1*). It entails the following aspects:

- Perform an endurance test campaign with a test rig specifically developed for the project.
- Develop a HM system able to detect degradations of the mechanical components (mainly the ballscrew transmission) before they will evolve into failures.

The need for a HM algorithm for flight EMAs is well motivated by previous substantial research efforts [20]. The Health On Line Monitoring for Electro-mechanical actuator Safety (HOLMES)-FP7 project [21] focused on developing fault detection and isolation (FDI) methods for EMAs mechanical components such as ballscrew transmission [22]–[25]. In the same way, the NASA funded several activities on fault diagnosis in aerospace using a flyable test-bed [26], [27]. A hybrid method, combining a signal-based and a knowledge-based method, based on machine learning classifiers, was proposed in [28]. Authors in [29] proposed a HM method for EMAs based on position predictive models. A model-based prognostic method for the freeplay identification in flight EMAs has been devised in [30]. Fault detection in aerospace EMAs for unmanned aerial system flight controls was proposed in [31]. Vibration symptoms of jam and metal flaking in the actuator ballscrew mechanism have been considered in [27]. Authors in [32] defined the structure that a knowledge-based approach to aerospace health monitoring, using expert systems, should have. Monitoring methods have been developed also for aircrafts hydraulic systems, see [33].

The *goal* of this paper is to *use Statistical Process Monitoring (SPM) methods for Health Monitoring of EMAs*.

SPM is used to perform Fault Diagnosis (FD) by applying multivariate statistics to industrial process data [34]. Typically, the Hotelling's T^2 statistic and the Q-statistic, also known as the Squared Prediction Error (SPE), are used for the detection of an out-of-control situation [35], [36]. Extension of the basic fault detection mechanism, like contribution and reconstruction plots, have been devised to accomplish also fault isolation and fault identification [34], [37].

However, fault diagnosis methods based on SPM look for a dichotomous answer, i.e. if there is an abnormal situation or not. This answer is *not suited for health monitoring*, since we need indicators that *continuously* evaluate the general health state of the system.

So, in this paper, we present a *general Health Monitoring approach* for *Electro-Mechanical Actuators* based on *Statistical Process Control methods*. The focus of the monitoring is on the mechanical transmission components, in particular, in the REPRISE project actuator, the ballscrew and nut assembly. The choice of using SPM methods over model-based approaches is due to the following facts:

- The design effort of HM indicators is lower for SPM approaches.

- Ability to capture the high-level, overall health state of the selected components, as opposed to focusing on their detailed behaviour.
- Difficulty to develop an adequate model of the system due to the limited number of measurable variables.

This paper presents the results of the first activity of the REPRISE project. The contributions are:

- To devise a methodology to *generate a set of Health Monitoring indicators* from the results of the SPM methods. As far as we are aware, this is the *first time* that such approach is proposed in literature.
- For HM, we employ *only standard measurements* (no additional sensors are used). In particular, we rely only on the EMA motor phase currents.
- The proposed method is *general* and *applicable to different types* of electro-mechanical actuators (also not in aerospace applications).
- We propose a preflight test strategy that employs the devised monitoring solution.
- We tested the method on a large dataset, *collected from a 1:1 scale EMA* for primary actuation of small aircrafts. To do this, we performed an extensive experimental activity, monitoring the actuator continuously.

The remainder of the paper is organized as follows. In section II, we show the results of a Failure Mode Effect and Criticality Analysis (FMECA) and a Fault Tree Analysis (FTA) on the tested EMA. Section III describes the experimental setup and the undergone test procedure. Section IV shows the results of visual inspections on the mechanical components of the EMA, i.e. the ballscrew. Section V describes the proposed general methodology, developing the health monitoring indicators. Section VI applies the method to the specific flight EMA. Finally, Section VII is devoted to conclusions and suggestions for future work.

ACRONYMS

A/C Aircraft
AEA All Electric Aircraft
HM Health Monitoring
EHSA Electro-HydroStatic Actuators
EMA Electro-Mechanical Actuators
FD Fault Diagnosis
MEA More Electric Aircraft
PBW Power-By-Wire
PCA Principal Component Analysis
SPM Statistical Process Monitoring

GLOSSARY

Health Monitoring A continuous real-time task of determining the health conditions of a physical system.

Failure Permanent interruption of a system/component ability to perform a required function under specified operating conditions.

Failure mode (ARP 1181A) A manner in which a device can or did fail. Simple devices may have only one failure mode; whereas, more complex devices can have several failure modes.

Failure Rate (MIL-F-9490D) The number of failures of an item per unit measure of life (flight, time, cycles, events, miles, etc) as applicable for the item.

Fault Unpermitted deviation of at least one characteristic property or parameter of a system from its acceptable/usual/standard condition. Failures and malfunctions originate from a fault.

Fault Diagnosis Determination of kind, size, location, time of occurrence of a fault and the fault signal. Fault diagnosis includes fault detection, isolation, estimation and identification.

Flight Hour Unit of measure of the time recorded in flight; generally reckoned from engine starting to shut-down.

Inspection Visual verification that the equipment as manufactured conforms to the design documentation.

Preflight Test A test that is administered on the ground and before every mission for the purpose of detecting latent failures

II. IDENTIFICATION OF THE MOST CRITICAL FAILURES

This section presents the reliability analysis performed in order to guide the experimental procedure design. Specifically, Failure Mode Effect and Criticality Analysis (FMECA) was performed to identify the actuator failure modes and their occurrence likelihood during a given mission profile. Then, exploiting the FMECA results, a Fault Tree Analysis (FTA) was performed to check if the existing actuator is compliant to the safety requirements.

A. FAILURE MODE EFFECT AND CRITICALITY ANALYSIS

The EMA used in this work consists of: (i) a BrushLess DC (BLDC) motor; (ii) a direct-drive nut-ballscrew transmission; (iii) an Electronic Control Unit (ECU), see Fig. 3.

This assembly was subject to a Failure Mode Effect and Criticality Analysis (FMECA), evaluating the failure mode rates of each single component according to the MIL-HDBK-217F handbook [38], over the mission profile reported in Table 1. The duration of the mission was one million of flight hours and the FMECA identified a total of 1950 different failure modes.

Table 2 shows the resulting Failure Mode Effect Summary (FMES): this table presents a summary of the identified equivalent failure modes rates, expressed as failures per million flight hours (fpmh). FMES results show that the majority of component failures do not compromise the overall system functionality. The results in Table 2 are then used as input to a Fault Tree Analysis (FTA), that will be used to *test the compliance of the considered EMA with the safety requirements defined by the project specifications*. For instance, the safety requirement on "Actuator runaway" in Table 3 depends on failure modes related to the static brake and loss of actuator reported in Table 2.

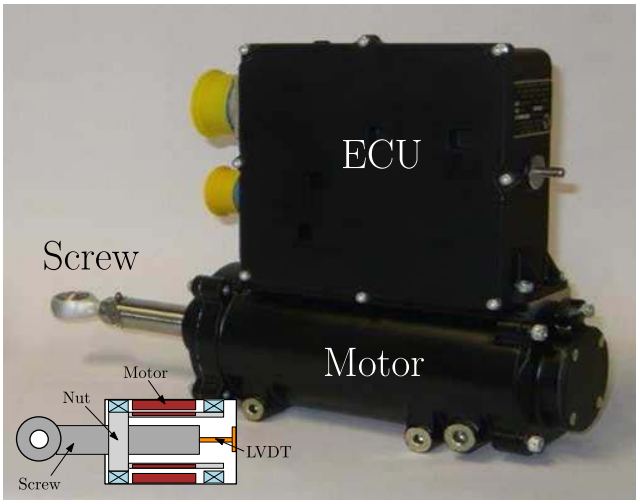

FIGURE 3. REPRISE EMA general view. The position of the direct-drive ballscrew transmission is measured by an internal LVDT sensor.

TABLE 1. Mission profile used for FMECA.

Mission phase	Percentage of mission duration	Temperature (C°)
A/C on ground and on takeoff	5%	+70
A/C on ground and on takeoff	2%	+85
Climb	6%	−15
Transfer and loiter	78%	−45
Descent	6%	−15
Landing	3%	+50

TABLE 2. Failure mode effect summary.

End effect	Failures per million hours (fpmh)
Actuator jam	$3.647 \cdot 10^{-2}$
Actuator runaway	$6.000 \cdot 10^{-6}$
False Alarm Signal	$7.859 \cdot 10^{-2}$
Loss of actuator	6.152
Loss of capability to engage the static brake	$3.664 \cdot 10^{-1}$
Loss of service communication	$5.748 \cdot 10^{-2}$
No functional effect	$1.039 \cdot 10^{1}$
No functional effect. The failure could become critical in presence of other failures	$1.777 \cdot 10^{-1}$
No significant effect	$4.366 \cdot 10^{-2}$
Possible loss of actuator	$1.550 \cdot 10^{-4}$
Static brake always engaged	$6.660 \cdot 10^{-2}$

B. FAULT TREE ANALYSIS

The fault tree analysis was performed to identify if the actuator is compliant to predefined safety requirements. FTA assessed four fundamental failure modes with their risk likelihood:

TABLE 3. Fault tree analysis summary.

Top FTA event	Risk likelihood (1/FH)	Requirement (1/FH)
Actuator loss of control/function	$6.218 \cdot 10^{-6}$	$< 10^{-7}$
Actuator free floating	$6.000 \cdot 10^{-9}$	$< 10^{-7}$
Actuator runaway	$2.0709 \cdot 10^{-12}$	$< 10^{-8}$
Actuator jam	$3.648 \cdot 10^{-8}$	$< 10^{-9}$

1) *Actuator loss of control/function*: the actuator is lost and cannot be controlled anymore. This event has been evaluated considering the combination in OR of all the failures leading to "Loss of Actuator". In particular, according to Table 2, the following failure mode end effects have been considered as causes for this event:
   a) Loss of actuator.
   b) Static brake always engaged.
   c) Possible loss of actuator.
2) *Actuator free floating*: the actuator results in free floating or excessive backlash, due to structural failures (e.g. the actuator is mechanically detached from the surface it controls). This is caused by breakage of physical structures.
3) *Actuator runaway*: the actuator results in free floating, hardover (deflection to an extreme position), uncommanded movements or oscillations, due to a failure in the actuator brake or erroneous readings from the motor position sensor. This event has been evaluated considering the following cases:
   a) The actuator has lost its functionality and it cannot be braked.
   b) The actuator makes a mistake in the evaluation of its position and moves in an incorrect position.

   In particular, case 3a has been considered as the combination in AND of: (i) actuator Loss of Control/Function and (ii) the actuator cannot be braked due to a failure of the brake assy or the loss of capability to command the actuator brake.
4) *Actuator jam*: there is a failure in the mechanisms related to the movement of the actuator, leading to actuator jamming. The considered components are the ballscrew, the nut and the bearings in the actuator assembly.

Table 3 shows the FTA results. The considered operational time for FTA is of 1 Flight Hour (FH). As can be noticed, *the safety requirements for failures 1) and 4) are not satisfied for the considered actuator*.

As a result of Table 3, we want to focus on failures with a risk likelihood higher than required by specifications. The actuator loss of control/function and jam failures can derive mainly from binding or breakage of the mechanical transmission, i.e. the ballscrew. One of the most plausible causes of the ballscrew damaging is the dwindling or contamination of the lubricant inside the ballscrew/nut assembly. Also, notice

TABLE 4. Aileron duty cycle.

Amplitude (% full range: 20.5 mm)	Load (% max load: 1346 N)	Cycles (per mission)	Cycles (total)
0.5	2.5	250.0	$2.17 \cdot 10^5$
1	1	4370.5	$3.80 \cdot 10^6$
1	5	100.0	$8.70 \cdot 10^4$
2.5	2.5	1984.0	$1.73 \cdot 10^6$
5	5	40.0	$3.48 \cdot 10^4$
5	25	2.0	$1.74 \cdot 10^3$
10	10	343.5	$2.99 \cdot 10^5$
25	10	0.0	$4.35 \cdot 10^0$
25	25	12.7	$1.10 \cdot 10^4$
50	25	4.0	$3.48 \cdot 10^3$
50	50	0.2	$1.74 \cdot 10^2$

TABLE 5. Elevator duty cycle.

Amplitude (% full range: 48.5 mm)	Load (% max load: 1405 N)	Cycles (per mission)	Cycles (total)
0.5	2.5	250.0	$2.17 \cdot 10^5$
1	2.5	4370.5	$3.80 \cdot 10^6$
1	5	100.0	$8.70 \cdot 10^4$
2.5	2.5	100.0	$8.70 \cdot 10^4$
2.5	5	1884.0	$1.64 \cdot 10^6$
5	5	40.0	$3.48 \cdot 10^4$
5	25	1.0	$8.70 \cdot 10^2$
10	10	0.4	$3.48 \cdot 10^2$
10	25	171.2	$1.49 \cdot 10^5$
25	50	7.4	$6.39 \cdot 10^3$
50	25	4.0	$3.48 \cdot 10^3$
50	50	1.0	$8.70 \cdot 10^2$

TABLE 6. Rudder duty cycle.

Amplitude (% full range: 47.4 mm)	Load (% max load: 1494 N)	Cycles (per mission)	Cycles (total)
0.5	10	250.0	$2.17 \cdot 10^5$
1	5	4370.5	$3.80 \cdot 10^6$
2.5	5	100	$8.70 \cdot 10^4$
2.5	50	2.0	$1.74 \cdot 10^3$
5	10	0.2	$1.74 \cdot 10^2$
5	25	343.3	$2.98 \cdot 10^5$
10	50	12.7	$1.10 \cdot 10^4$
50	25	4.0	$3.48 \cdot 10^3$
50	100	0.2	$1.78 \cdot 10^2$

that, while possible during the operating life of the EMA, the lack of lubricant is more plausibly due to a maintenance error. So, the experimental conditions were designed in order to evaluate the requirements not satisfied in Table 3 (see Section III-B).

The experimental activity, described in the following Section III, is specifically conceived to collect data for developing the monitoring algorithms with specific attention to the critical failures of the ballscrew/nut assembly, as evidenced above.

C. PERFORMANCE REQUIREMENTS AND DESIGN OF EXPERIMENTS

In order to design the experimental activity for the realization of the Health Monitoring algorithm, it is of paramount importance to know the performance requirements that the available EMA has been designed to fulfil, so that it will be possible to perform tests which can bring to system degradation (in addition to evaluate its current health status). The considered EMA has been designed according to specifications about:

(i) *dynamic properties* of the control system (i.e. closed loop bandwidth and tracking error), not reported for confidentiality reasons, but considered in the design of experiments;
(ii) *physical characteristics* of the assembly (i.e. mass, overall dimensions), also confidential but not limiting the design of experiments;
(iii) *nominal operating conditions*: the EMA is also required to comply with predefined *duty cycles* for each of the actuated primary flight control (aileron, elevator, rudder).

Tables 4, 5, 6 show the duty cycles for the primary controls, where:

- *Full range* refers to the surface full deflection (Aileron: 20.5 mm, Elevator: 48.5 mm, Rudder: 47.4 mm);
- *Max load* is the largest rated *axial load* (Aileron: 1346 N, Elevator: 1405 N, Rudder: 1494 N). The EMA is required to tolerate a *radial load* up to 17% of the axial load;
- The EMA has to be able to perform such duty cycles, with a *sinusoidal position profile* with amplitude given by the *amplitude* column of the Tables 4, 5, 6, and a frequency between 0.2 Hz and 1 Hz.

From Tables 4, 5, 6 it can be noticed that *the most demanding condition is the rudder configuration* (in terms of combined axial force and stroke). This worst-case configuration is taken as a guide for the experimental campaign design.

It is also worth noting that the EMA, for the most time of its life, actuates a very little range (less than 1 mm) with a very small load (less than 150 N). So, the experiments will be designed taking into account this feature, but also considering that using sinusoidal profiles with higher amplitudes, i.e. 5 mm and 10 mm, will accelerate the test times leading to earlier observation of a degradation in the system. Experimental setup and performed tests will be described in the next section.

III. EXPERIMENTAL LAYOUT AND TESTING PROCEDURE DEFINITION

Following the results of the failure analysis of the previous section, there are two ways to increase the compliance to not satisfied requirements: (i) design an enhanced actuator (phase 2 of the REPRISE project); (ii) embed the EMA with a monitoring software that can assess the system state and prevent the appearance of a failure (phase 1 of the REPRISE project and *focus of this paper*). In order to design a HM algorithm, an extensive experimental activity has been devised with two main goals: (i) to induce accelerated degradation of

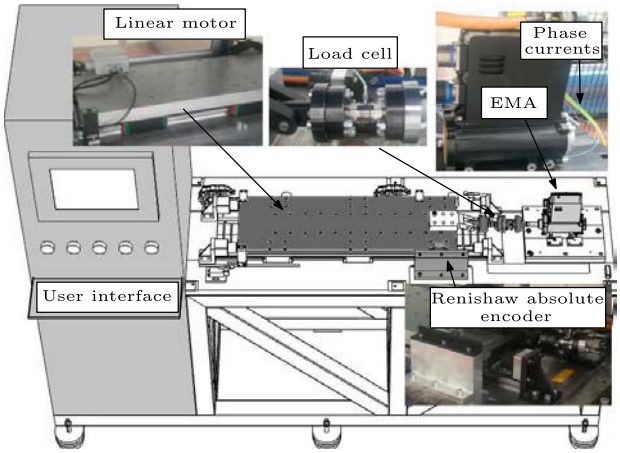

FIGURE 4. Test bench with main components.

the EMA, accordingly with the conclusions of the previous section; (ii) to periodically evaluate the EMA health status.

This section discusses the experimental activity carried out on the available EMA. The aim is to progressively lead the actuator to failure by means of an ''Endurance'' test activity. Data are collected to characterize the system and the degradation behaviour. In the following, we will describe: (i) the experimental setup and the measured variables; (ii) the chosen test procedure; (iii) a summary of the performed tests.

A. EXPERIMENTAL LAYOUT

The EMA is installed in a test bench suitably designed to provide the desired load and the actuator position reference trajectories, see Fig. 4. The test rig is endowed with additional external sensors in order to monitor the system status.

1) EMA DESIGN

The EMA is composed by a BrushLess Direct Current (BLDC) electric motor, an Electronic Control Unit (ECU) and a ballscrew (see Section II-A and Fig. 3). The BLDC motor is a 3-phases Brushless DC motor with 5 poles. Two 28 Vdc power supplies are used to power a single DC bus, so that the actuator is able to operate even when one electric power supply is missing. The ECU also hosts current, speed and position closed-loop controllers. The position measure comes from three Hall sensors and an embedded LVDT transducer. The EMA can travel up to ± 30 mm from its centered position (position offset equal to 0 mm). The ballscrew transmission consists of 8 circuits with 1 turn each and a specific number of balls per turn (not specified for confidential reasons). Moreover, in its standard operating conditions, the EMA is endowed with an anti-rotation device which is able to compensate small radial load components. *We considered tests with and without this component.*

2) LOAD GENERATION

The load on the actuator is generated by a Parker Ironcore R16-3A-HS linear motor controlled by a force closed-loop controller; this control loop uses a piezoelectric Kistler 9321BU load cell to feed back the measured load. The test bench has a Renishaw Resolute absolute optical encoder to measure the EMA absolute position; this sensor is used to evaluate the position controller performance and it is not used in the actuator position control system. Finally, three LEM ATO-20-B333-D10 sensors, that enclose the phase currents cables, are used to sense the 3 motor phase currents. This is necessary because the motor ECU cannot save the current internal measurements. Finally, the EMA is placed inside an air-cooled box to keep its temperature at standard room values.

3) CONTROL AND USER INTERFACES

The supervision and management software of the test bench is realized in National Instruments Labview and it is deployed on a National Instrument (NI) cRIO 9030. The cRIO generates the force and position reference signals. The cRIO uses the force measure fed back by the load cell to compute the load control command. This command is sent to the linear motor drive, that generates the control action to actuate the linear motor. The position control loop is managed by the ECU of the EMA, which gets the position reference from the cRIO and implements three cascaded control loops (position, speed and current). The software exposes a user interface where it is possible to insert the test parameters. Furthermore, it is also responsible for collecting measurements from the control chain. Finally, it is possible to configure the bench software to one of the aforementioned applicative settings, i.e. aileron, elevator and rudder. As said in Section II, *we used the rudder configuration of the test rig* to carry out the tests. It is worth noting that, in this configuration, the software is designed to provide only *sinusoidal position reference trajectories*. This follows from the specifications given in Table 6.

The physical variables, collected by the cRIO described above and a NI cDAQ 9188, are:

1) Linear motor load reference.
2) Temperature inside the EMA box.
3) Current supplied to the EMA (from power supply)
4) Load cell measure.
5) EMA position reference.
6) EMA position measure from (embedded) LVDT sensor.
7) EMA position measure from (external) absolute optical sensor.
8) Current supplied to the linear motor (from its drive).
9) EMA 3-phase currents.

The data are sampled at 100 Hz, but for the phase currents (sampled at 4800 Hz). An example of measured data is shown in Fig. 5.

B. TESTING PROCEDURE

As already said, the goal of the tests is twofold: (i) to stress the actuator with tests in operating conditions suitable to lead the ballscrew to mechanical degradation and, eventually, to jamming, while (ii) providing measurements useful to

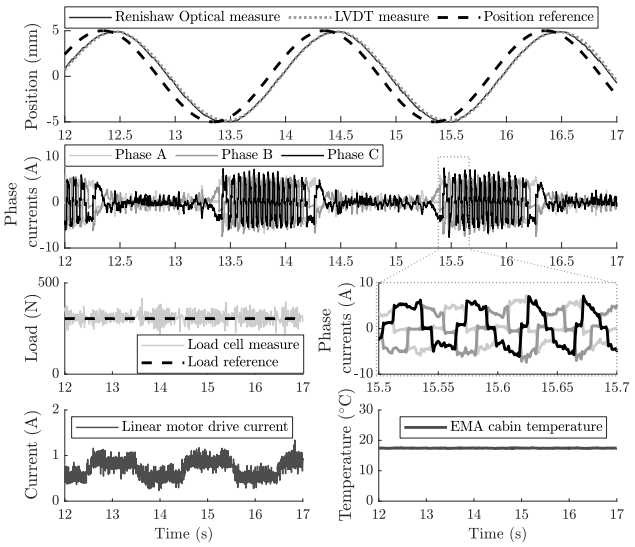

FIGURE 5. Examples of measurements from the test bench. Sine frequency: 0.5 Hz. Position amplitude: 10 mm. Load: 300 N. The phase currents plot has been zoomed, in order to see the currents behaviour.

continuously monitor the health state of the ballscrew, using the proposed algorithm.

1) DESIGN OF EXPERIMENTS

In order to obtain the aforementioned goals, an alternation of two kinds of trials was used:

(i) *Monitoring trials*, designed to acquire the measurements necessary to evaluate the health status of the EMA.
(ii) *Endurance trials*, designed to gradually deteriorate the ballscrew components by "over-stressing" them using suitable load and suitable reference trajectories.

These two kinds of tests alternate, providing both periodic continuous monitoring of the ballscrew conditions and worsening of the system conditions. Specifically, the Monitoring trials have been performed 16 times, from April 2017 to October 2017. Between two consecutive Monitoring trials, Endurance trials are performed.

As specified above, in the rudder configuration, the EMA can be commanded only by sinusoidal position reference. So, an experiment is completely defined by the frequency, amplitude and offset of the position reference trajectory.

A total of 10 frequency values are used (in Hz): {0.1, 0.3, 0.5, 0.8, 0.9, 1, 1.5, 2, 2.5, 4}. This range was chosen according to the designed position tracking bandwidth of the EMA. For each frequency value, we tested the amplitude and offset values described in Table 7. So, an *experimental session* consists of repeating the 6 test configurations of Table 7 for each of the 10 frequency values defined above. Usually, a Monitoring trial consists in executing one experimental session, while Endurance trials consist in repeating many successive identical experimental sessions.

TABLE 7. Position configurations in the experimental table.

Offset position (mm)	Amplitude position (mm)	Stroke range (mm)	N° of cycles
0	5	$[-5, +5]$	100
0	10	$[-10, +10]$	100
+10	5	$[+5, +15]$	100
+10	10	$[0, +20]$	100
−10	5	$[-15, -5]$	100
−10	10	$[-20, 0]$	100

Notice that the EMA total stroke range during the tests is $[-20, +20]$ mm. According to Table 6 this represents the stroke value of about the 99.9% of the total cycles.

The axial load conditions were chosen based on: (i) the requirements of Table 6; (ii) the pressure experienced by the balls in the ballscrew at those loads.

According to Table 6, in the 99.6% of the total cycles the aerodynamical load is smaller than 373 N, which is about the 25% of the maximum rated load of 1494 N. For this reason, we used a load of 300 N as the *nominal H0 load test condition*.

2) EXPERIMENTAL CONDITIONS

The *experimental conditions* have been defined to accelerate the system failure, i.e. the ballscrew/nut assembly degradation process. Specifically, the following actions have been undertaken:

- Employing 3 circuits out of 8 in the ballscrew.
- Removing EMA anti-rotation device (after an initial test period).
- Radial load equal to 17% of axial load.
- Progressively remove lubricant in ballscrew/nut assembly.

We employed *only* 3 *circuits out of the* 8, which is the design value. In this way, the load is sustained by a smaller number of balls. In addition, after the initial test phase, *the anti-rotation device was removed*. These expedients lead to a greater force acting on the balls and ballscrew tracks, creating an harsher condition for the EMA.

Also, we configured the bench such that a radial load, proportional to the axial load, is generated. Specifically, the radial load is 17% of the applied axial load, i.e. the maximum radial load imposed by the EMA design requirements.

Recall that, as discussed in section II, we want to focus on failures of the ballscrew and the main possible cause of degradation is the lack of lubricant. For this reason (and also to accelerate the EMA damaging) we tested the EMA in three different operating conditions:

1) *Normal lubricant*: standard level of lubricant.
2) *Poor lubricant*: lubricant partially removed (about half).
3) *No lubricant*: lubricant completely removed.

In all the cases, the temperature of the test bench cabin, where the EMA resides, was kept approximately constant (at ambient temperature) by means of an air-cooling system (see Fig. 5). For each of the listed conditions, Monitoring

and Endurance trials are performed as described in the next paragraphs.

3) FINITE ELEMENT ANALYSIS

A major factor for ballscrew deterioration is the force acting on the recirculating balls. In order to estimate this force, a Finite Element Method (FEM) analysis has been performed to assess at which load an overstressed condition of the ballscrew is present. We denote a condition as *over-stressing* if at least one ball is subject to a force greater than an assigned nominal value N_0 N (the value N_0 is not shown for confidential reasons). Otherwise, we say that the system is in a *nominal* load condition.

First of all, the FEM analysis was performed *before the anti-rotation device removal* in three load conditions: 300 N, 800 N and 1200 N. In these settings, we identified that at 300 N of axial force, no ball was over-stressed. At 800 N and 1200 N, more than one ball is over-stressed.

The FEM analysis was performed also *without the anti-rotation device*. Fig. 6 depicts the computed force on each ball, for three balls circuits. It can be observed that, also in this case, no ball is over-stressed with 300 N load. In the other load conditions, there are over-stressed balls. However, pressures at 1200 N load were too high and so, after anti-rotation removal, the tests were performed only at 800 N load.

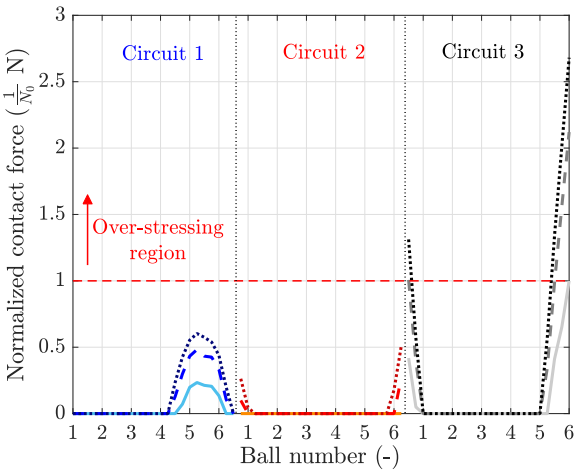

FIGURE 6. Simulated force on the balls in the three recirculation circuits. Axial load: 300 N (solid line), 800 N (dashed line), 1200 N (dotted line). Circuit 1 (blue), Circuit 2 (red), Circuit 3 (black). The number of balls shown does not reflect reality, and units are normalized for confidential reasons.

Concluding, *Monitoring trials were executed at a load of* 300 N (nominal H0 condition); *Endurance trials were performed with loads of* 800 N (over-stressed H1 condition) *and* 1200 N (over-stressed H1b condition - only *before* anti-rotation removal).

C. TEST REPORT

The tests were performed from April 2017 to October 2017 (see Table 8 where the number of cycles refers to the number of periods of sinusoidal profiles executed). The traveled distance is computed by taking into account the amplitude of the reference position and an estimate of the position closed-loop transfer function. The estimation of the Frequency Response Function (FRF) has been performed by sine sweeps at 0 N of reference load (Other loads condition). Fig. 7 presents a complete test summary during time. Some dates, when we performed Monitoring trials, are highlighted (in some dates we performed more than one Monitoring trial). The anti-rotation device was removed after an initial test phase, since no evident actuator degradation were observed (visually and from data).

Fig. 8 depicts the travelled distance and the screw revolutions (drawn in the plot) considering only tests after anti-rotation removal. The tests performed between 11 and 18 Sept. 2017 were all with normal lubrication. After that, tests were performed by gradually removing lubricant. The dates evidenced in the plot refer to Monitoring trials execution. It is useful to remind that, between a Monitoring trial and another, Endurance trials were executed to stress the actuator. For the algorithm evaluation, Monitoring trials from 18 Sept. 2017 to 12 Oct. 2017 were considered. It is worth noting

TABLE 8. Tests summary.

Load condition	N of cycles	Work time (h)	Distance (km)	Number of revolutions
H0: 300 N	324.882	164, 88	8, 20	2.582.939
H1: 800 N	644.010	324, 74	16, 29	5.130.369
H1b: 1200 N	249.200	95, 00	5, 87	1.850.274
Other loads	248.037	71, 68	11, 85	3.732.531
Total	**1.466.129**	**656, 30**	**42.21**	**13.296.113**

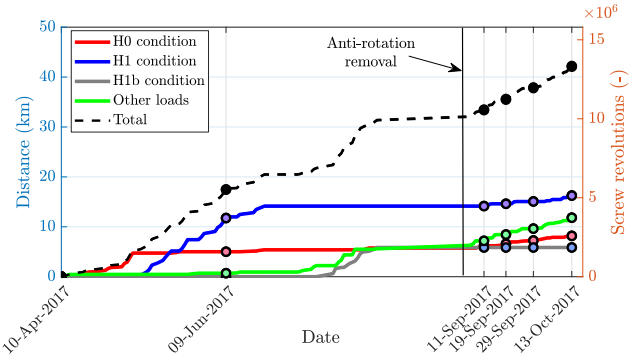

FIGURE 7. Graphical representation of performed tests during time.

TABLE 9. Number of screw revolutions after anti-rotation removal.

	Normal lubricant	Poor lubricant	No lubricant	**Total**
H0: 300 N	185.609	250.388	333.023	**769.020**
H1: 800 N	146.846	145.212	371.579	**663.637**
Total	**332.455**	**395.600**	**704.602**	**1.432.657**

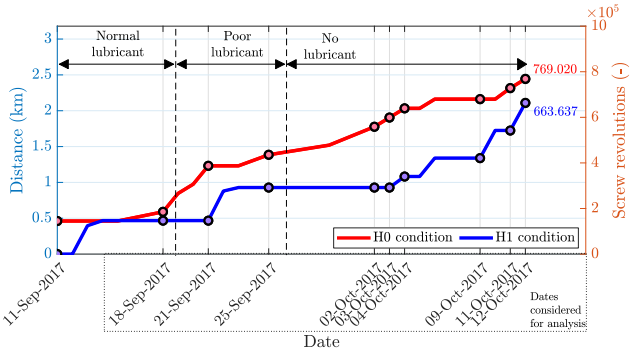

FIGURE 8. Graphical representation of performed tests during time, after anti-rotation removal.

FIGURE 9. Visual inspection at 01 September 2017. Balls of third circuit (a) and screw shaft (b). The components do not show degradation.

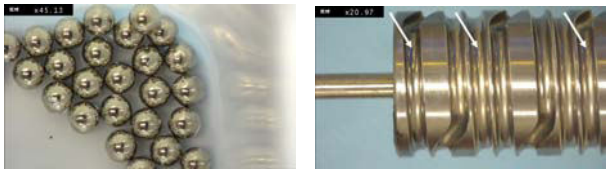

FIGURE 10. Visual inspection at 13 October 2017. Balls of third circuit (a) and screw shaft (b). The balls show "hammer-blow" signs. The screw threads show signs of wear (white arrows).

that, few days after 13 Oct. 2017, the mechanical transmission underwent a mechanical jam, *reaching a complete failure*.

IV. VISUAL INSPECTION RESULTS

This section describes qualitative evaluations regarding the health state of the balls and the screw threads. After each Monitoring test the ballscrew was disassembled and the balls and the screw threads where visually inspected, in order to verify the real state of degradation of the mechanical transmission. At the end of the test campaign, the screw thread deformation was also measured with a profilometer.

The inspections on balls and screw threads were performed at various stages between September 2017 and October 2017. Fig. 9 depicts pictures of the balls and of the screw shaft at 01 September 2017 and no sign of degradation is visible. Fig. 10 shows the same components during the tests without lubricant. The balls show a strong degradation of their surface, with typical "hammer-blow" signs. The screw threads show evident dark scrapes. The reason for this is that the balls, due to the high pressure on them, are no more rolling but they are sliding for the most of their time.

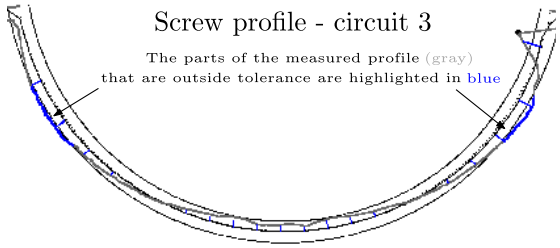

FIGURE 11. Profile of the screw thread in one of the areas of higher contact pressure (third circuit). The thread profile is deeper than the ideal one (in places pointed out by arrows).

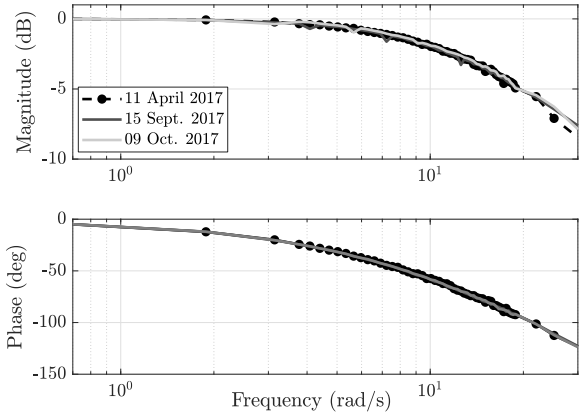

FIGURE 12. Bode diagrams of the position closed-loop system. No difference is visible through time.

The visual inspection data are confirmed by a quantitative measurement of the deformation of the screw thread profile. This was measured by means of a profilometer Mitutoyo CV 3200 H4. The tolerance bands on profiles are of ± 0.05 μm. Fig. 11 reports the profile measurement for the third screw thread (the one with higher contact pressures, see Fig. 6). The regions where balls, due to the high pressures, delved into the screw are evidenced in the plot by arrows.

Last but not least, it is worth stressing that, during all the tests, *the motor correctly performed its function*, i.e. the position tracking was correctly performed in all test conditions, notwithstanding the mechanical degradation evidenced by the above described analysis. Fig. 12 reports the Bode plots resulting from this analysis at three different dates: (i) before anti-rotation removal - 11 April 2017; (ii) just after anti-rotation removal - 15 Sept. 2017, (iii) during no lubricant tests - 09 Oct. 2017. The plot shows how the frequency response of the EMA did not change significantly. So, in order to design a Health Monitoring algorithm detecting a degradation in the system, it is necessary to resort to "internal" variables, such as the phase currents (the control actions).

V. HEALTH MONITORING ALGORITHM

This section presents an algorithm for continuous Health Monitoring of EMAs. The algorithm is based on *Statistical*

Process Monitoring (SPM) ideas and it provides a set of *indicators* that have well defined stochastic properties and can be easily used for the health state assessment of the ballscrew/nut assembly.

SPM has the *Fault Detection* (FD), not Health Monitoring (HM), as its main goal. In this work, *we adapt the SPM Fault Detection approach to Health Monitoring needs*, by using a wise method for the thresholds assignments and the definition of *indicators* that can be used (jointly or alone) for a quantitative evaluation of the system health conditions. Moreover, having the time history of the indices it is possible to estimate the *Remaining Useful Life* (RUL) of the system by extrapolation.

Results of the application of this method to the REPRISE project EMA will be presented in section VI and it is worth noting that the results provided by the algorithm are in strong agreement with the visual inspection results presented in the previous section IV.

First, we review basic notation and results from the process monitoring field [37], [40]. Let $\mathbf{x} \in \mathbb{R}^{n\times 1}$ be a sample vector of n variables. Given m observations, a data matrix $\mathbf{X} \in \mathbb{R}^{m\times n}$ can be defined as

$$\mathbf{X} = [\mathbf{x}(1) \quad \mathbf{x}(2) \quad \dots \quad \mathbf{x}(m)]^\top. \tag{1}$$

From now on, we suppose that data in matrix $\mathbf{X}$ have been normalized to zero mean and unit variance, using sample estimates of the mean and variance of each of the n variables. The covariance of $\mathbf{x}$ is approximated by the sample covariance matrix

$$\mathbf{S} \approx \frac{1}{m-1}\mathbf{X}^\top\mathbf{X}. \tag{2}$$

Principal Components Analysis (PCA) is used to decompose $\mathbf{S}$ as

$$\mathbf{S} = \mathbf{P}\Lambda\mathbf{P}^\top + \tilde{\mathbf{P}}\tilde{\Lambda}\tilde{\mathbf{P}}^\top = \hat{\mathbf{S}} + \tilde{\mathbf{S}}, \tag{3}$$

where $\hat{\mathbf{S}} = \mathbf{P}\Lambda\mathbf{P}^\top$ and $\tilde{\mathbf{S}} = \tilde{\mathbf{P}}\tilde{\Lambda}\tilde{\mathbf{P}}^\top$. Here $\mathbf{P} \in \mathbb{R}^{n\times l}$ and $\tilde{\mathbf{P}} \in \mathbb{R}^{n\times(n-l)}$ contain the principal and residual orthonormal *loading vectors*, respectively, with l denoting the number of Principal Components (PCs) retained by the model. Diagonal matrices $\Lambda \in \mathbb{R}^{l\times l}$ and $\tilde{\Lambda} \in \mathbb{R}^{(n-l)\times(n-l)}$ contain the *principal eigenvalues set* $\hat{\mathcal{S}} = \{\sigma_i\}_{i=1,\cdots,l}$ and the *residual eigenvalues set* $\tilde{\mathcal{S}} = \{\tilde{\sigma}_i\}_{i=l+1,\cdots,n}$, respectively. The most popular statistical indices used in SPM fault detection are the Squared Prediction Error (SPE) and the Hotelling's T^2 statistics [36].

A. SQUARED PREDICTION ERROR (SPE) INDEX OR Q STATISTIC

The SPE index, also know as Q statistic, is defined as:

$$Q \equiv \| \left(\mathbf{I} - \mathbf{P}\mathbf{P}^\top\right)\mathbf{x}\|_2^2. \tag{4}$$

For an assigned confidence level $(1-\alpha)\times 100\%$, the threshold for the SPE index can be computed as $\rho^2 = g^{\mathrm{SPE}}\chi^2_\alpha\left(h^{\mathrm{SPE}}\right)$ with $g^{\mathrm{SPE}} = \frac{\theta_2}{\theta_1}$, $h^{\mathrm{SPE}} = \frac{\theta_1^2}{\theta_2}$, $\theta_j = \sum_{i=l+1}^{n}\tilde{\sigma}_i^j$, where $\tilde{\sigma}_i \in \tilde{\mathcal{S}}$ is the i-th eigenvalue of $\mathbf{S}$, and $\chi^2_\alpha\left(h^{\mathrm{SPE}}\right)$ is the h^{SPE} degrees of freedom Chi-squared distribution deviate, corresponding to the $(1-\alpha)$ percentile [37]. Further improvements for the SPE bounds can be found in [34].

B. HOTELLING'S T^2 STATISTICS

The T^2 index is defined as

$$T^2 \equiv \mathbf{x}^\top\mathbf{P}\Lambda^{-1}\mathbf{P}^\top\mathbf{x} = \mathbf{x}^\top\mathbf{D}\mathbf{x}, \tag{5}$$

where $\mathbf{D} = \mathbf{P}\Lambda^{-1}\mathbf{P}^\top \in \mathbb{R}^{n\times n}$ is a positive semidefinite matrix computed using $\mathbf{P}$ and Λ defined above. A process is said to be in *nominal conditions* when $T^2 \le \tau^2$, where $\tau^2 = \frac{l(m-1)(m+1)}{m(m-l)}F_\alpha(l, m-l)$[1] is a positive threshold value. Here, $F_\alpha(l, m-l)$ indicates the deviate corresponding to the $(1-\alpha)$ percentile of a F-distribution with l and $m-l$ degrees of freedom, see [34]. Notice that both T^2 and τ^2 are strictly greater than zero if $m > 1$ and $\mathbf{x} \neq 0$.

C. FAULT DETECTION USING Q AND T^2 STATISTICS

The use of Q and T^2 for Fault Detection consists in a two-step procedure. First of all, a *training or set-up phase* of the FD algorithm is performed, using data measured in "nominal", i.e. no fault, condition (*training data*). Then, the FD algorithm is ready to be used on new data sets (*test data*). The procedure is summarized in Algorithm 1.

Algorithm 1 Fault Detection With Q and T^2 Statistics

Input: Training and test data, l, α
Output: Presence or absence of a fault

Training or set-up phase:
1. normalize training data to zero mean and unit variance
2. using l, compute the matrices $\mathbf{P}$, Λ and $\tilde{\Lambda}$
3. using α, compute the ρ^2 and τ^2 thresholds

Test phase:
4. normalize test data using the same mean and variance used in step 1
5. compute the statistics (4) and (5) on the normalized test data using $\mathbf{P}$, Λ and $\tilde{\Lambda}$ computed in step 2
6. compare each statistic with its threshold: if its value exceed the threshold, then a fault is detected in the process data and an alarm is raised

Finally, notice that both these indices depend on tuning parameters. Specifically, both of them depend on the choice of l, i.e. the dimension of the PC subspace and on the confidence level α. Obviously, the smaller is α, the larger will be the thresholds τ^2 and ρ^2 and so it is less likely to have crossings. For instance, as a consequence, the false alarm rate

[1] In the cases that the covariance matrix is estimated from data and they are assumed to follow a multivariate Gaussian distribution.

will be decreased. The number of PCs l that are retained is guided by the amount of the variance of the data that is explained. This parameter can be tuned, for instance, on the basis of the S/N ratio in the measurements.

D. SPM FOR HEALTH MONITORING OF AN ELECTRO-MECHANICAL ACTUATOR

We now present the main contribution of the paper, i.e. a general method for Health Monitoring of EMAs. The algorithm can be applied to any electromechanical system to evidence degradation mainly in the mechanical components (e.g. the transmission). The approach is based on the computation of *numerical indicators*, based on Q and T^2 indices, using the actuator control action, i.e. the motor phase current measurements. This choice is based on the assumption that the system will lose efficiency as degradation worsen and larger control action would be required to perform the same task, even though there is no external evident effect of degradation. In fact, the EMA control system is generally able to compensate for degradation hiding its effects (see Section IV).

The algorithm processes phase current measurements taken during periodic tests along the lifetime of the actuator. For instance, in the case of an airplane actuator, the data can be measured during a preflight test or a periodic maintenance test performed every assigned flight hours number.

The algorithm outline is the following:

1) Denote with $\mathbf{i}_t^{(i)} \in \mathbb{R}^{m\times 1}$ for $i = 1, \cdots, p$ the vectors containing the p phase currents measurements in the t-th experimental periodic test. Here, m indicates the number of sampled data with sampling time T_s during the t-th test.
   The $t = 0$-th test is the *training data set* which is reserved to compute the normalization mean and variance and the thresholds τ^2 and ρ^2, for a given α value.
2) Then, the data matrix $\mathbf{X}_t \in \mathbb{R}^{m\times(p-1)}$ is constructed as follows, $\forall t$:

$$\mathbf{X}_t = \begin{bmatrix} \mathbf{i}_t^{(1)} & \mathbf{i}_t^{(2)} \cdots \mathbf{i}_t^{(p-1)} \end{bmatrix} = \begin{bmatrix} \mathbf{x}_t(1)^\top \\ \vdots \\ \mathbf{x}_t(m)^\top \end{bmatrix}, \tag{6}$$

   where each variable $\mathbf{x}_t(j) \in \mathbb{R}^{(p-1)\times 1}$, $j = 1, \ldots, m$ is such that $\mathbf{x}_t(j) = \begin{bmatrix} \mathbf{i}_t^{(1)}[j] & \mathbf{i}_t^{(2)}[j] \cdots \mathbf{i}_t^{(p-1)}[j] \end{bmatrix}^\top$, and $\mathbf{i}_t^{(i)}[j]$ is the j-th component of the vector $\mathbf{i}_t^{(i)}$, $i \in \{1, \ldots, p-1\}$.
   The choice of using only $p-1$ phase currents is due to the fact that only $p-1$ of them are linearly independent, as the phase currents sum to zero at each time instant in BLDC motors.
3) Following the SPM rationale presented in Algorithm 1, the next step is to perform PCA on $\mathbf{X}_t$, retaining a number of components l such that a given fraction of the variance of the data is explained. Usually, l is chosen so that 90% of the variance is explained, but a different value can be chosen depending on the S/N ratio in the available measurements.
4) Then, compute the $Q_t(j)$, $T_t^2(j)$ values, one for each observation $\mathbf{x}_t(j)$, which will be used to create the monitoring indicators. The computed values $Q_t(j)$ and $T_t^2(j)$ must be compared to the corresponding thresholds ρ^2 and τ^2, previously computed using the training data set.
5) Each threshold violation define an *event* $e_t(j)$ s.t. for $j = 1, \ldots, m$:

$$e_t(j) = \begin{cases} 1 & \text{if } T_t^2(j) > \tau^2 \\ 0 & \text{if } T_t^2(j) \le \tau^2 \end{cases} \tag{7}$$

   and similarly for the Q statistic. We assume that *a lower system health leads to a higher number of threshold violations*.
6) The event vector is used to compute ***four health monitoring indicators***. They use the dichotomous (discrete) notion of an event to produce an index that is amenable to a continuous health assessment.

   (i) **Event frequency**.
   The *event frequency* indicator λ_t is defined as the percentage of observed events N_t over the number of data m in an observation time t_e with sampling time T_s, s.t. $m = t_e \cdot 1/T_s$ and $N_t = \sum_{j=1}^{m} e_t(j)$:

$$\lambda_t = \frac{\#\text{ of events}}{\#\text{ of data}} \cdot 100\% \equiv \frac{N_t}{m} \cdot 100. \tag{8}$$

   (ii) **Mean time to event**.
   The *mean time to event* (MTTE) indicator Δ_t computes the average time that lasts between any two consecutive events. We call these quantities *inter-arrival times*. With N_t events, there are $N_t - 1$ inter-arrival times. Define with $K \subset \mathbb{N}$ the ordered set (in increasing order) of indices j s.t. $e_t(j) = 1$. Let the number of observations between event i and event $i+1$, with $i = 1, \ldots, N_t - 1$, be $\delta_{i,t} = \left(k_{i+1} - k_i\right)$, with $k_i \in K$ the index when event i occurs. The indicator Δ_t is therefore computed as

$$\Delta_t = \frac{\text{sum of inter-arrival times}}{\#\text{ of inter-arrival times}} \equiv \frac{\sum_{i=1}^{N_t-1} \delta_{i,t}}{N_t - 1} \cdot T_s. \tag{9}$$

   (iii) **Weibull distribution of inter-arrival times rising edges**
   The Weibull distribution is a vastly employed tool in reliability engineering and survival analysis for modeling random variables that represent *times* [41]. In particular, when the modeled variables consist of "time-to-failure" data, the Weibull distribution is used to model the *failure rate* of the components subject to failure and it can be expressed as [41]:

$$w(x|\beta, \eta) = \frac{\beta}{\eta}\left(\frac{x}{\eta}\right)^{\beta-1} \cdot \exp\left[-\left(\frac{x}{\eta}\right)^{\beta}\right], \tag{10a}$$

$$W(x|\beta,\eta) = 1-\exp\left[-\left(\frac{x}{\eta}\right)^{\beta}\right], \tag{10b}$$

where $x \in \mathbb{R}_{\geq 0}$ represent time-to-failure data, $w(\cdot)$, $W(\cdot)$ are the probability density function and cumulative density function respectively, $\beta > 0 \in \mathbb{R}$ is the *shape parameter*, $\eta > 0 \in \mathbb{R}$ is the *scale parameter*. Then, the following quantities can be computed:

$$h(x|\beta,\eta) = \frac{w(x)}{1-W(x)} = \frac{\beta}{\eta}\left(\frac{x}{\eta}\right)^{\beta-1}, \tag{11a}$$

$$S(x|\beta,\eta) = 1 - W(x) = \exp\left[-\left(\frac{x}{\eta}\right)^{\beta}\right], \tag{11b}$$

where $h(\cdot)$ is the *hazard function* or instant failure rate, and $S(\cdot)$ is the *survivor (or survival) function*.

The shape parameter β characterises the aging property of the components. In particular, we have [41]:

- Negative aging if $\beta < 1$, indicates that the failure rate decreases over time.
- Non-aging if $\beta = 1$, indicates that the failure rate is constant over time. It is equal to employ an exponential distribution.
- Positive aging if $\beta > 1$, indicates that the failure rate increases with time, which is appropriate for modelling wear-out failure due to gradual deterioration/degradation of an item over time.

As the considered *component degrades*, we expect that:

- The average time-to-failure *gets lower*, since we expect an impending failure. We call this quantity *life expectancy*.
- The standard deviation of the times-to-failure *gets lower*, since we are more confident about the imminent event. We call this quantity *life expectancy awareness*.

These rationales are condensed in the features of the Weibull distribution parameters that can be used to create two Health Monitoring indicators, exploiting the events $e_t(j)$ defined above.

First of all, define as *rising edge* the first event $e_t(j)$ of a continuous chain of succeeding events (i.e. a successive strike of $e_t(j) = 1$ values). Then, store the times between consecutive rising edges in the variables $r_t(z)$ and $z = 1, \ldots, R_t$ with R_t the number of rising edges in experimental test t. Values in $r_t(z)$ are the *time-to-failure* data. Thus, we fit a Weibull distribution via maximum-likelihood to this data.

The maximum-likelihood estimates of the Weibull parameters, using the data data $r_t(z)$, indicated as $\hat{\eta}_t$ and $\hat{\beta}_t$, are the last two indicators.

Remark. The choice of using only times between rising edges is due to to the fact that we could have long strikes of events for which $e_t(j) = 1$. In this case, most of the data (i.e. number of observations between event i and $i+1$) are concentrated at the value of $\delta_{i,t} = 1$. This is detrimental for the estimate of a distribution from time-to-failure observation. Using falling edges instead of rising ones yields analogous results.

Remark. When the observation time ends before observing the event of interest, we have a so-called *right-censored value*. In our case, censored data appear only if the events strike last until the end of the experiment. In this case, the last rising edge does not have a corresponding "next rising edge". We considered the measured number of observation as a censored data. The fit of the Weibull parameters accounts for this information.

7) Each indicator can be interpreted by looking at:
   - *relative variations*, i.e. changes in its value over time
   - *absolute variations*, i.e. comparing its value to an assigned "warning" threshold.

   Considering the last case, it is worth noting that these indicators, thanks to their properties, have "natural" thresholds. When the event frequency $\hat{\lambda}_t$ is above 50 %, more than half of the data are above threshold. The MTTE Δ_t has a natural lower limit that is the sampling time T_s. In this case, all the data are above threshold. So, a threshold can be put at $2T_s$. When the Weibull shape parameter $\hat{\beta}_t$ is greater than 1, we have positive aging, that means that the failure rate is increasing with time. The Weibull scale parameter $\hat{\eta}_t$ depends in a non-trivial way from data. Since it is more complicated to set an absolute value for a threshold, it can be useful to look at relative variations, e.g. when it reaches -50% of its first value. Obviously, the user can use these indicators in different ways according to the application features.

As a consequence, different use strategies of the indicators are possible. For instance, a warning can be raised only when all the indicators crossed their own threshold or, when only one among them crossed its own, or a majority of them did. Also, a subset of indicators can be computed, for instance only those based on the T^2, like in the application case of this paper, or based on a combination of T^2 and SPE [37]. Notice that the indicators 1 and 3 in (8) and (9) are very simple to compute, while accurate estimation of the Weibull parameters requires an optimization process. Furthermore, indicator 1 in (8) and indicator 3 in (9) represents very similar information: from a practitioner point of view, it is possible to implement just one of them. These choices depend on the application field and the safety requirements.

The proposed HM approach is summarized in Algorithm 2, for a specific test t.

VI. APPLICATION RESULTS AND DISCUSSION

This section shows the results obtained by applying the procedure described in Section V to the datasets acquired during the Monitoring trials highlighted in Fig. 8, using the REPRISE three phase EMA described in section III.

Algorithm 2 Health Monitoring With Q and T^2 Statistics for a Single Test t

Input: $\mathbf{i}_t^{(1)}, \mathbf{i}_t^{(2)}, \ldots, \mathbf{i}_t^{(p-1)}, l, \alpha$
Output: t-th value of the four HM indicators
compute $\mathbf{X}_t$ in (12)
Training or set-up phase (for $t = 0$):
run steps 1-2-3 of Algorithm 1$(\mathbf{X}_0, l, \alpha)$ to compute $\rho^2, \tau^2, \mathbf{P}, \Lambda, \tilde{\Lambda}$
Training or set-up phase (for $t > 0$):
run steps 4-5 of Algorithm 1$(\mathbf{X}_t, l, \alpha)$ to compute $e_t(j)$ in (7), for $j = 1, \ldots, m$
compute $\lambda_t, \Delta_t, \hat{\eta}_t, \hat{\beta}_t$

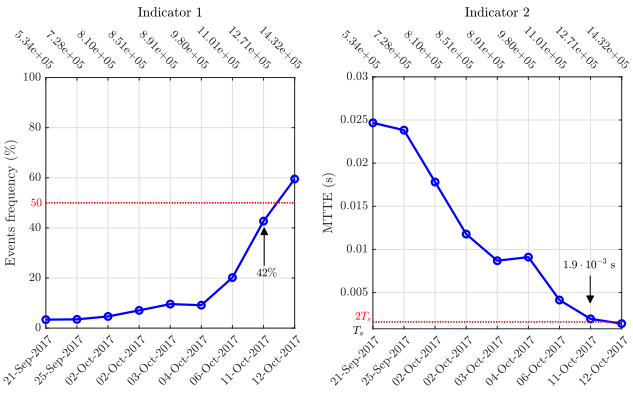

FIGURE 13. Indicator 1 λ_t and Indicator 2 Δ_t computed on Monitoring trials, as function of test dates (bottom axis) and total number of screw revolutions after anti-rotation removal (top axis).

Furthermore, a comparison with a different rationale from [42], based on a change detection algorithm that also relies on the motor phase currents, is provided.

A. PROPOSED METHOD

The proposed indicators are computed using Monitoring trials data, from Sept. 21, 2017 to Oct. 12, 2017, see Fig. 8. In this dates range, there are $T = 9$ datasets. The dataset of Sept. 18, 2017, i.e. the last dataset in healthy condition, is used as the $t = 0$ dataset (the *training dataset*), in order to tune the alarm thresholds and to compute the normalization mean and variance. The confidence interval is $\alpha = 0.05$. For each of the 9 datasets, one value of four indicators is computed, using the T^2 index. Therefore, we have 9 values for each indicator.

The current measurements were downsampled by a factor of 4 to speed up the computations. So, the new sampling time of the data is therefore $T_s = 1200$ Hz. This operation does not affect the dynamics of the phase currents. The data consist of tests at 0 mm offset and 10 mm amplitude. This choice approximates the motor usage described in Table 6: (i) the actuator usually starts from the 0 mm offset position; (ii) the 10 mm of amplitude span most of the useful stroke of the actuator. This is also the condition that could be easily used in a periodic preflight or maintenance test. The dataset were measured with position closed loop control using sinusoidal reference trajectories at different frequency values, as specified in section III-B. Each experiment was 90 s long and the first 10 s were discarded to remove transients and initial conditions effects.

The data matrix $\mathbf{X}_t$ of the t-th Monitoring trial is computed using two out of three phase currents $\mathbf{i}_t^{(b)}, \mathbf{i}_t^{(c)}$ for $t = 1, \ldots, 9$. So, the data matrix $\mathbf{X}_t \in \mathbb{R}^{m\times 2}$ is, $\forall t$:

$$\mathbf{X}_t = \begin{bmatrix} \mathbf{i}_t^{(b)} & \mathbf{i}_t^{(c)} \end{bmatrix}. \tag{12}$$

In particular, the vectors $\mathbf{i}_t^{(b)}, \mathbf{i}_t^{(c)}$ in (12) are defined as follows. Let $F = \{f_1, f_2, \ldots, f_{n_f}\}$ be a set of n_f frequencies. Denote with $\mathbf{i}_{f,t}^{(b)}, \mathbf{i}_{f,t}^{(c)} \in \mathbb{R}^{m\times 1}$ the vectors containing the phase currents measurements in the t-th Monitoring trial, at a frequency f of the sinusoidal reference position profile s.t. $f \in F$, for the two motor phases b, c respectively. Now, compute the quantities $\mathbf{i}_t^{(p)} \in \mathbb{R}^{m\times 1}, p \in \{b, c\}$, as the sum of two phase currents across all considered set of frequencies F:

$$\mathbf{i}_t^{(p)} = \sum_{f\in F} \mathbf{i}_{f,t}^{(p)}. \tag{13}$$

The set of considered frequencies in (13) is (in Hertz) $F = \{0.3, 0.5, 0.8, 0.9, 1\}$. This is a subset of $n_f = 5$ frequencies from the 10 frequencies used to perform Endurance and Monitoring trials, see Section III-B. The choice of the frequencies in F is motivated by the requirements described in Section II-C.

In this specific case, the data matrix has two columns that are linearly independent, so the SPE index cannot be computed and only the T^2 index is used. Here, using a 90% threshold of explained variance in PCA ensures that, if one of the two phase currents signals is faulty (e.g. due to a broken sensor), the method will discard the noise component and maintains the signal component.

The computed indicators are depicted in Fig. 13 and Fig. 14. All the indicators show a fast evolving trend starting when the lubricant has been reduced and then eliminated. Also, a quite monotonic behaviour has been obtained, in line with the progressive degradation of the actuator.

The *Event frequency* indicator λ_t shows an exponential increase of the percentage of events with actuator degradation. A warning threshold can be set when a certain chosen percentage level is reached. In Fig. 13 the 50% threshold is evidenced. Remember that, in the case of complete failure of the actuator, this indicator will reach the value of 100%. However, in the experimental tests performed, no failure happened and at the end of the tests the system closed loop position control was providing good performance (see section IV).

The *MTTE* indicator Δ_t shows a decreasing behaviour of the mean time between events, as expected. Since the pre-processed data have a sampling time of about $T_s \approx 8 \cdot 10^{-4}$ s, by the end of the tests, approximately 1 every 10 measurements generates an event. Again, a threshold can

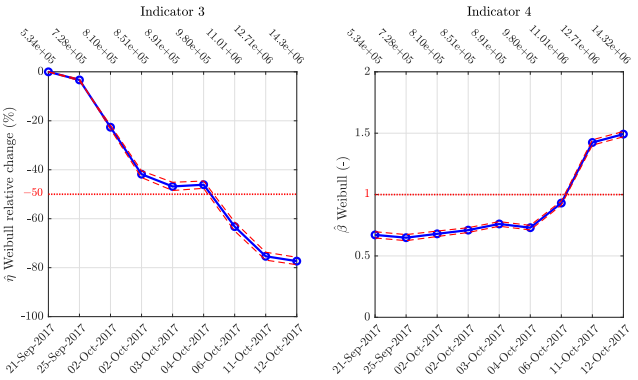

FIGURE 14. Indicator 3 $\hat{\eta}_t$ (percentage change with respect to first value) and Indicator 4 $\hat{\beta}_t$ computed on Monitoring trials, as function of test dates (bottom axis) and total number of screw revolutions after anti-rotation removal (top axis). Confidence intervals on estimates are shown (dashed red lines).

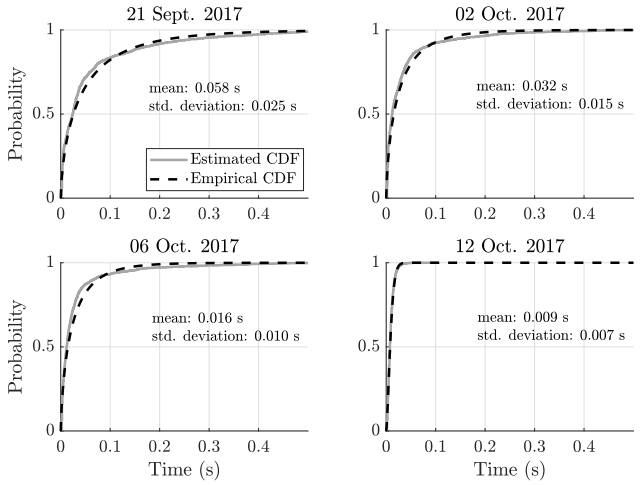

FIGURE 15. Estimated Weibull cumulative density functions (gray line) and empirical distribution from data (dashed black line), for different Monitoring trials, with respective mean values and standard deviations.

be set to raise a warning when the mean time to event gets too low. In case of complete failure, the MTTE will be equal to T_s.

The *Weibull shape parameter* indicator $\hat{\beta}_t$ and *Weibull scale parameter* indicator $\hat{\eta}_t$ are depicted with the 95% confidence intervals on the parameters estimates. The index $\hat{\eta}_t$ is reported as percentage change with respect to the value $\hat{\eta}_1$. As the motor degrades, more rising edges are present. Therefore, the estimates are more certain and confidence intervals get narrower. A warning level for $\hat{\beta}_t$ can be automatically computed noting that, when $\hat{\beta}_t > 1$ (i.e. the failure rate increases with time), it is possible to say that the actuator is starting to degrade. Fig. 14 shows how this value is approached by the test of 06 Oct. 2017 and exceeded by the test of 11 Oct. 2017, accordingly with the other indicators. Indicator $\hat{\eta}_t$ depends in a non-trivial way from data, so it is more complicated to set a threshold. However, one can raise an alarm when its value is, for example, less than 50% of its first value $\hat{\eta}_1 = 0.044$, resulting in a threshold of 0.022. Again, this is true for the test of 11 Oct. 2017.

The behaviour of $\hat{\eta}_t$ and $\hat{\beta}_t$ can be better understood by computing the mean value and standard deviation of the resulting Weibull distributions (one for each test). Fig. 15 depicts the empirical and estimated cumulative density functions $W(x|\beta_t, \eta_t)$, see (10b). It can be seen how the mean value (*life expectancy*) and the standard deviation (*life expectancy awareness*) of the estimated models decrease with degradation. This means that the times between rising edges are getting shorter and shorter, and there is less and less uncertainty about their value.

Remark: The proposed rationale implicitly assumes that test conditions are equal to those used for setting the τ^2 threshold. In fact, one can imagine that phase currents varies with a different load than the nominal one used when setting τ^2. For this reason, the proposed approach can be used when the aircraft is on ground, for example during a preflight test, when load conditions are supposed to be the same.

B. COMPARISON WITH A METHOD BASED ON CHANGE DETECTION

In this section, we compare the proposed approach with the one outlined in [42]–[44], based on a *change detection* method. We choose this method for a comparison because: (i) it is a data-driven batch approach, although based on the evaluation of completely different statistical indicators; (ii) it makes use of the motor phase currents for monitoring, as the proposed methodology. Here the aim is to look for *statistical changes in the distribution of the data*, from one experiment to another. In this sense, the method in [42] works in a *batch* fashion, as the one proposed in this work. The rationale is to estimate the $\tilde{\alpha}$-relative Pearson divergence [42] between the distributions of the data sets from the two experiments that are compared, with $\tilde{\alpha} \in \mathbb{R}$ an hyperparameter of the method. The output is an indication of "dissimilarity" of the two experiments. The divergence is computed by estimating the *ratio* of the two data distributions (one for each test) through a parametric linear combination of Gaussian densities.

The data considered in [42] are the Root Mean Square (RMS) and Crest Factor (CF) features computed from the same phase currents signals of the BLDC motor considered in this work. Given a test with sinusoidal input profile and a fixed frequency of movement, these two features are computed with the three phase currents data for each period of the sinusoidal input. So, we have that each test is represented by a feature matrix $\mathbf{Z}_t \in \mathbb{R}^{2\times 100}$, i.e. two features and 100 input sinusoidal periods (cycles), see Table 7.

The rationale for computing the health monitoring indicator is as follows [42]. First, in the set-up phase, compute the divergence π_0 between two healthy tests. We consider as the $t = 0$ test the experiment on 11 Sept. 2017, and as $t = 1$ test the experiment on 18 Sept. 2017, see Fig. 8. Then, set a threshold ξ as two-times π_1. The subsequent tests are then compared with the last experiment $t = t^*$ that exceeded the

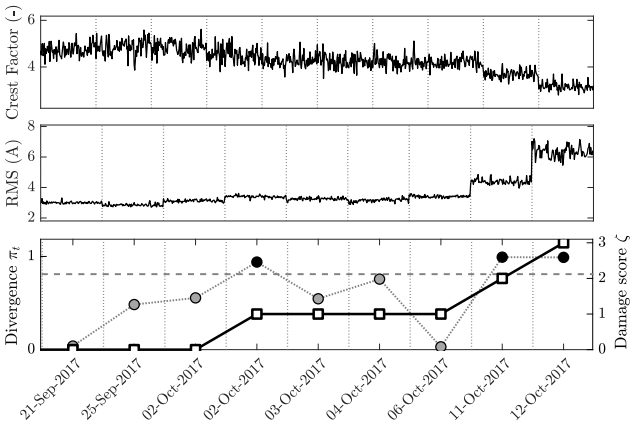

FIGURE 16. Results of the change detection method of [42] for an input sinusoidal profile at 1 Hz, 300 N load and 10 mm stroke. (Top) Crest factor values. (Middle) RMS values. (Bottom) computed divergence π_t (gray and black dots) and monitoring score ζ (white squares).

threshold ξ. Each time ξ is violated, a damage counter ζ is incremented. The algorithm is summarized in Algorithm 3 and the results are reported in Fig. 16 for a fixed frequency of 1 Hz, a 300 N load and a 10 mm stroke as in [42].

Algorithm 3 Health Monitoring With Change Detection

Input: $\mathbf{Z}_{t^*}$, $\mathbf{Z}_t$, hyperparameters vector ψ
Output: t-th value of the damage indicator ζ

Training or set-up phase (for $t \leq 1$):
compute the divergence π_1 between $\mathbf{Z}_0$ and $\mathbf{Z}_1$
set a threshold $\xi \leftarrow 2 \cdot \pi_1$

Test phase (for $t > 1$):
$\zeta \leftarrow 0; \quad t^* \leftarrow 1$
compute the divergence π_t between $\mathbf{Z}_{t^*}$ and $\mathbf{Z}_t$
if $\pi_t > \xi$ **then**
  $t^* \leftarrow t; \quad \zeta \leftarrow \zeta + 1$
end

C. DISCUSSION

As can be seen in Figures 13, 14 and 16, both approach are able to assess the motor degradation before the end of the motor life. In this regard, the proposed indicators admits a more intuitive threshold definition, upon which its crossing denotes an "alarm" condition. In the method of [42], the damage score ζ monotonically increases but it is difficult to define a proper threshold to trigger and alarm.

The proposed approach needs the definition of only two parameters: (i) the confidence level α and the number of principal components l (or a percentage of explained variance). The method of [42] requires the tuning of three hyperparameters: (i) the $\tilde{\alpha}$ term; (ii) a regularization term μ and (iii) the standard deviation of the Gaussian components ι. While, in principle, both sets of hyperparameters could be tuned by some cross-validation procedure, in the proposed approach their tuning is less critical and more interpretable.

Furthermore, for the specific applicative case considered, the proposed approach is able to take into consideration more frequencies of motion (remember that the reference position is sinusoidal), while the method in [42] is constrained to consider only a single input frequency.

VII. CONCLUDING REMARKS AND FUTURE DIRECTIONS

A. CONCLUDING REMARKS

This paper presented the results of the REPRISE project in developing a Health Monitoring approach for Electro-Mechanical Actuators. An extended experimental activity has been carried out on a 1:1 scale EMA, by means of a test rig specifically designed for this project. Dynamic, load and operating conditions were defined on the basis of the flight actuator requirements and reliability analysis. Wear was induced in the EMA transmission by lubricant gradual removal. Since the actuators are usually closed-loop controlled, the monitoring approach is based on the analysis of the control actions, i.e. the motor phase currents. Relying on methods borrowed from the statistical process control literature, that generally give a dichotomous output, we defined a set of monitoring indicators suited to assess continuously the overall health state of the actuator. We tested the proposed general approach on an EMA employed for the actuation of primary flight control surfaces in small aircrafts. Although the proposed approach rely on the assumption that the external conditions (load, disturbances) remain the same during all the test sessions, it can be effectively employed as a preflight test procedure or a periodic maintenance operation.

B. FUTURE DIRECTIONS

The method envisioned in this paper is a knowledge-based one, i.e. it relies on a batch of previously acquired data to set the value of statistic thresholds. As already mentioned, the assumption about stationarity of the external conditions has to be made for this approaches to remain valid through different times and experiments. A model-based approach, if feasible, would permit to decouple disturbances and noise from actual inputs, being therefore robust against external variations. However, a proper model-based scheme requires specific conditions on the number of measured inputs/outputs with respect to the number of faults/disturbances to be managed, see [45], that are not always satisfied. Obviously, a model of the system has to be developed, with its difficulties such as non-linearities and time-varying behaviours. A Model-based approach is therefore a sought next direction to be investigated, that could bring noticeably improvements. Further work is also envisioned in order to test the repeatability of the results shown in this paper.

REFERENCES

[1] J. A. Rosero, J. A. Ortega, E. Aldabas, and L. Romeral, "Moving towards a more electric aircraft," *IEEE Aerosp. Electron. Syst. Mag.*, vol. 22, no. 3, pp. 3–9, Mar. 2007.

[2] W. Cao, B. C. Mecrow, G. J. Atkinson, J. W. Bennett, and D. J. Atkinson, "Overview of electric motor technologies used for more electric aircraft (MEA)," *IEEE Trans. Ind. Electron.*, vol. 59, no. 9, pp. 3523–3531, Sep. 2012.

[3] A. L. Cologni, M. Mazzoleni, and F. Previdi, "Modeling and identification of an electro-hydraulic actuator," in *Proc. 12th IEEE Int. Conf. Control Autom. (ICCA)*, Jun. 2016, pp. 335–340.

[4] G. Qiao, G. Liu, Z. Shi, Y. Wang, S. Ma, and T. C. Lim, "A review of electromechanical actuators for more/all electric aircraft systems," *J. Mech. Eng. Sci.*, vol. 232, no. 22, pp. 4128–4151, 2018.

[5] Y. Zhang, G. O. H. Peng, J. K. Banda, S. Dasgupta, M. Husband, R. Su, and C. Wen, "An energy efficient power management solution for a fault-tolerant more electric engine/aircraft," *IEEE Trans. Ind. Electron.*, vol. 66, no. 7, pp. 5663–5675, Jul. 2019.

[6] D. Belloli, F. Previdi, S. M. Savaresi, A. Cologni, and M. Zappella, "Modeling and identification of an electro-hydrostatic actuator," *IFAC Proc. Vol.*, vol. 43, no. 18, pp. 620–625, 2010.

[7] W. J. Norton, "Advanced electromechanical actuation system (EMAS), flight test," Wright-Patterson Air Force Base, Dayton, OH, USA, Tech. Rep. AD-A176-148b, Jun. 1986. [Online]. Available: https://apps.dtic.mil/dtic/tr/fulltext/u2/a176148.pdf

[8] S. C. Jensen, G. D. Jenney, and D. Dawson, "Flight test experience with an electromechanical actuator on the F-18 systems research aircraft," in *Proc. 19th DASC Digit. Avionics Syst. Conf.*, vol. 1, Oct. 2000, pp. 2E3/1–2E3/10.

[9] M. Hirst, A. Mcloughlin, P. J. Norman, and S. J. Galloway, "Demonstrating the more electric engine: A step towards the power optimised aircraft," *IET Electr. Power Appl.*, vol. 5, no. 1, pp. 3–13, 2011.

[10] T. Jomier. (Dec. 2009). *Final Report Summary*. [Online]. Available: https://trimis.ec.europa.eu/sites/default/files/project/documents/20121218_094726_85827_MOET_Public_Technical_report.pdf

[11] J. Derrien, P. Tieys, D. Senegas, and M. Todeschi, "EMA aileron COVADIS development," SAE Tech. Paper 2011-01-2729, 2011.

[12] (2016). *Final Report Summary*. [Online]. Available: https://cordis.europa.eu/project/rcn/101114/reporting/en

[13] J. W. Bennet, "Fault tolerant electromechanical actuators for aircraft," Ph.D. dissertation, School Elect., Electron. Comput. Eng., Newcastle Univ., Newcastle, U.K., 2010.

[14] T. Nelson. (2005). *787 Systems and Performance*. [Online]. Available: http://myhres.com/Boeing-787-Systems-and-Performance.pdf

[15] J. Fu, J.-C. Maré, and Y. Fu, "Modelling and simulation of flight control electromechanical actuators with special focus on model architecting, multidisciplinary effects and power flows," *Chin. J. Aeronaut.*, vol. 30, no. 1, pp. 47–65, 2017.

[16] D. Crane, *Dictionary of Aeronautical Terms*. Newcastle, WA, USA: Aviation Supplies & Academics, 2006.

[17] G. Buticchi, L. Costa, and M. Liserre, "Improving system efficiency for the more electric aircraft: A look at DC\/DC converters for the avionic onboard DC microgrid," *IEEE Ind. Electron. Mag.*, vol. 11, no. 3, pp. 26–36, Sep. 2017.

[18] G. Gong, M. L. Heldwein, U. Drofenik, J. Minibock, K. Mino, and J. W. Kolar, "Comparative evaluation of three-phase high-power-factor AC-DC converter concepts for application in future more electric aircraft," *IEEE Trans. Ind. Electron.*, vol. 52, no. 3, pp. 727–737, Jun. 2005.

[19] M. Mazzoleni, Y. Maccarana, F. Previdi, G. Pispola, M. Nardi, F. Perni, and S. Toro, "Development of a reliable electro-mechanical actuator for primary control surfaces in small aircrafts," in *Proc. IEEE Int. Conf. Adv. Intell. Mechatronics (AIM)*, Jul. 2017, pp. 1142–1147.

[20] M. Todeschi and L. Baxerres, "Health monitoring for the flight control EMAs," *IFAC-PapersOnLine*, vol. 48, no. 21, pp. 186–193, 2015.

[21] (2017). *Final Report Summary*. [Online]. Available: https://cordis.europa.eu/project/rcn/110748/reporting/en

[22] M. Villani, M. Tursini, G. Fabri, and L. Castellini, "High reliability permanent magnet brushless motor drive for aircraft application," *IEEE Trans. Ind. Electron.*, vol. 59, no. 5, pp. 2073–2081, May 2012.

[23] M. Mazzoleni, G. Maroni, Y. Maccarana, S. Formentin, and F. Previdi, "Fault detection in airliner electro-mechanical actuators via hybrid particle filtering," *IFAC-PapersOnLine*, vol. 50, no. 1, pp. 2860–2865, 2017.

[24] M. Mazzoleni, Y. Maccarana, and F. Previdi, "A comparison of data-driven fault detection methods with application to aerospace electro-mechanical actuators," *IFAC-PapersOnLine*, vol. 50, no. 1, pp. 12797–12802, 2017.

[25] M. Mazzoleni, S. Formentin, F. Previdi, and S. M. Savaresi, "Fault detection via modified principal direction divisive partitioning and application to aerospace electro-mechanical actuators," in *Proc. IEEE 53rd Annu. Conf. Decis. Control (CDC)*, Dec. 2014, pp. 5770–5775.

[26] E. Balaban, A. Saxena, S. Narasimhan, I. Roychoudhury, M. Koopmans, C. Ott, and K. Goebel, "Prognostic health-management system development for electromechanical actuators," *J. Aerosp. Inf. Syst.*, vol. 12, no. 3, pp. 329–344, 2015.

[27] M. A. A. Ismail, E. Balaban, and H. Spangenberg, "Fault detection and classification for flight control electromechanical actuators," in *Proc. IEEE Aerosp. Conf.*, Mar. 2016, pp. 1–10.

[28] A. J. Chirico, III, and J. R. Kolodziej, "A data-driven methodology for fault detection in electromechanical actuators," *J. Dyn. Syst. Meas. Control. Trans. ASME*, vol. 136, no. 4, p. 041025, 2014.

[29] G. Di Rito and F. Schettini, "Health monitoring of electromechanical flight actuators via position-tracking predictive models," *Adv. Mech. Eng.*, vol. 10, no. 4, 2018, Art. no. 1687814018768146.

[30] G. Di Rito, F. Schettini, and R. Galatolo, "Model-based prognostic health-management algorithms for the freeplay identification in electromechanical flight control actuators," in *Proc. 5th IEEE Int. Workshop Metrol. Aerosp. (MetroAeroSpace)*, Jun. 2018, pp. 340–345.

[31] G. Di Rito, F. Schettini, and R. Galatolo, "Model-based health-monitoring of an electro-mechanical actuator for unmanned aerial system flight controls," in *Proc. IEEE Int. Workshop Metrol. Aerosp. (MetroAeroSpace)*, Jun. 2017, pp. 502–511.

[32] P. Phillips and D. Diston, "A knowledge driven approach to aerospace condition monitoring," *Know.-Based Syst.*, vol. 24, no. 6, pp. 915–927, Aug. 2011.

[33] J. P. P. Gomes, L. R. Rodrigues, B. P. Leão, R. K. H. Galvão, and T. Yoneyama, "Using degradation messages to predict hydraulic system failures in a commercial aircraft," *IEEE Trans. Autom. Sci. Eng.*, vol. 15, no. 1, pp. 214–224, Jan. 2018.

[34] E. L. Russell, L. H. Chiang, and R. D. Braatz, *Data-Driven Methods for Fault Detection and Diagnosis in Chemical Processes*. London, U.K.: Springer-Verlag, 2012.

[35] S. J. Qin, "Survey on data-driven industrial process monitoring and diagnosis," *Annu. Rev. Control*, vol. 36, no. 2, pp. 220–234, Dec. 2012.

[36] S. Yin, S. X. Ding, X. Xie, and H. Luo, "A review on basic data-driven approaches for industrial process monitoring," *IEEE Trans. Ind. Electron.*, vol. 61, no. 11, pp. 6418–6428, Nov. 2014.

[37] C. F. Alcala and S. J. Qin, "Reconstruction-based contribution for process monitoring," *Automatica*, vol. 45, no. 7, pp. 1593–1600, Jul. 2009.

[38] (1995). *Reliability Prediction of Electronic Equipment*. [Online]. Available: https://snebulos.mit.edu/projects/reference/MIL-STD/MIL-HDBK-217F-Notice2.pdf

[39] F. Previdi and T. Parisini, "Model-free actuator fault detection using a spectral estimation approach: The case of the DAMADICS benchmark problem," *Control Eng. Pract.*, vol. 14, no. 6, pp. 635–644, 2006.

[40] S. J. Qin, "Statistical process monitoring: Basics and beyond," *J. Chemometrics*, vol. 17, nos. 8–9, pp. 480–502, 2003.

[41] R. Jiang and D. N. P. Murthy, "A study of Weibull shape parameter: Properties and significance," *Rel. Eng. Syst. Saf.*, vol. 96, no. 12, pp. 1619–1626, 2011.

[42] M. Mazzoleni, M. Scandella, Y. Maccarana, F. Previdi, G. Pispola, and N. Porzi, "Condition monitoring of electro-mechanical actuators for aerospace using batch change detection algorithms," in *Proc. IEEE Conf. Control Technol. Appl. (CCTA)*, Aug. 2018, pp. 1747–1752.

[43] F. Previdi, Y. Maccarana, M. Mazzoleni, M. Scandella, G. Pispola, and N. Porzi, "Development and experimental testing of a health monitoring system of electro-mechanical actuators for small airplanes," in *Proc. 26th Medit. Conf. Control Autom. (MED)*, Jun. 2018, pp. 673–678.

[44] M. Mazzoleni, M. Scandella, Y. Maccarana, F. Previdi, G. Pispola, and N. Porzi, "Condition assessment of electro-mechanical actuators for aerospace using relative density-ratio estimation," *IFAC-PapersOnLine*, vol. 51, no. 15, pp. 957–962, 2018.

[45] A. Varga, *Solving Fault Diagnosis Problems*, vol. 84. Springer, 2017.

MIRKO MAZZOLENI (M'18) was born in Ponte San Pietro, Italy, in 1989. He received the M.Sc. degree *(summa cum laude)* in computer engineering and the Ph.D. degree in engineering and applied sciences (control systems) from the University of Bergamo, Italy, in 2014 and 2018, respectively. He is currently an Assistant Professor with the University of Bergamo. His main research interests include system identification, machine learning, and fault diagnosis.

FABIO PREVIDI (M'10) was born in Milan, Italy, in 1968. He received the M.Sc. degree in electronic engineering (control systems) and the Ph.D. degree in control systems engineering from the Politecnico di Milano, Milan, in 1993 and 1999, respectively, and the M.Sc. degree in physics from the University of Milan, in 2008. From 1999 to 2000, he was a Research Assistant with the Centre for Systems and Control, Department of Mechanical Engineering, University of Glasgow, Glasgow, U.K. From 2000 to 2002, he was a Research Assistant with the Politecnico di Milano. From 2002 to 2006, he was an Assistant Professor with the Engineering Faculty, University of Bergamo, Dalmine, Italy, where, in 2006, he became an Associate Professor, and, in 2017, a Full Professor of control systems. His research interests include fault diagnosis, system identification, control of biomedical systems, and industry applications of control systems methods.

MATTEO SCANDELLA was born in Clusone, Italy, in 1992. He received the M.Sc. degree *(summa cum laude)* in computer engineering from the University of Bergamo, in 2016, where he is currently pursuing the Ph.D. degree in engineering and applied sciences (control systems). His main research interests include system identification and fault detection.

GIULIO PISPOLA was born in Perugia, Italy, in 1978. He received the M.Sc. degree in mechanical engineering, in 2003, and the Ph.D. degree in industrial engineering from the University of Perugia, in 2006. Since 2006, he has been with Umbra Group S.p.A., Foligno, where he was an Research and Development Project Manager and is currently a Material and Process Engineer.